J. Fluid Mech. (1986), *vol.* 167, *pp.* 65–93
Printed in Great Britain

A study of singularity formation in a vortex sheet by the point-vortex approximation

By ROBERT KRASNY
Courant Institute of Mathematical Sciences, New York University, NY 10012, USA

(Received 3 February 1984 and in revised form 9 November 1985)

The initial-value problem for perturbations of a flat, constant-strength vortex sheet is linearly ill posed in the sense of Hadamard, owing to Kelvin–Helmholtz instability. Previous numerical studies of this problem have experienced difficulty in converging when the mesh was refined. The present work examines Rosenhead's point-vortex approximation and seeks to understand better the source of this difficulty. Using discrete Fourier analysis, it is shown that perturbations introduced spuriously by computer roundoff error are responsible for the irregular point-vortex motion that occurs at a smaller time as the number of points is increased. This source of computational error is controlled here by using either higher precision arithmetic or a new filtering technique. Computations are presented which use a linear-theory growing eigenfunction of small amplitude/wavelength ratio as the initial perturbation. The results indicate the formation of a singularity in the vortex sheet at a finite time as previously found for other initial data by Moore and Meiron, Baker & Orszag using different techniques of analysis. Numerical evidence suggests that the point-vortex approximation converges up to but not beyond the time of singularity formation in the vortex sheet. For large enough initial amplitude, two singularities appear along the sheet at the critical time.

1. Introduction

The vortex sheet is an asymptotic model of a parallel shear flow in which the thickness of the transition region between the two streams is small compared with a typical streamwise lengthscale. As a step towards determining the extent to which this idealized model can describe properties of a real flow, the present work studies a discretization of the model and also touches on some of the model's properties. Specifically, we shall examine Rosenhead's point-vortex approximation for vortex-sheet evolution from periodic analytic initial data.

1.1. *The analytic initial-value problem*

A vortex sheet in two-dimensional ideal flow can be described by a complex curve,

$$z(\Gamma,t) = x(\Gamma,t)+\mathrm{i}y(\Gamma,t), \tag{1.1}$$

where t is time and Γ is a Lagrangian parameter which measures the circulation between a base point $\Gamma = 0$ and an arbitrary point along the sheet (Birkhoff 1962). The vortex-sheet strength $\sigma(\Gamma,t)$ is the jump in tangential velocity across the sheet and is determined by $\sigma(\Gamma,t) = |z_\Gamma|^{-1}$ where $z_\Gamma = \partial z/\partial\Gamma$. Consider a vortex sheet

for which $p(\Gamma,t) = z(\Gamma,t)-\Gamma$ is periodic in Γ with period 1. The initial-value problem to be studied is,

$$\frac{\partial \bar{z}}{\partial t}(\Gamma,t) = \frac{1}{2\mathrm{i}} \fint_0^1 \cot \pi(z(\Gamma,t)-z(\tilde{\Gamma},t))\,\mathrm{d}\tilde{\Gamma}, \tag{1.2a}$$

$$z(\Gamma,0) = \Gamma+p(\Gamma,0). \tag{1.2b}$$

The bar over z on the left side of (1.2a) denotes complex-conjugate and the slash on the integral sign denotes Cauchy principal value. Equation (1.2a) is the kinematical condition that the vortex sheet move with the fluid. The dynamical requirement that circulation around material curves be preserved is contained in the statement that Γ is a Lagrangian variable. Initial condition (1.2b) is a perturbation of the flat vortex sheet of constant strength $z(\Gamma,t) = \Gamma$ which is an equilibrium solution of (1.2a).

Linear stability analysis of this equilibrium yields perturbation solutions proportional to $\exp 2\pi(\omega t+\mathrm{i}k\Gamma)$ when the dispersion relation

$$\omega^2 = \tfrac{1}{4}k^2, \tag{1.3}$$

is satisfied (Batchelor 1967). For each wavenumber $k > 0$ there is a growing and a decaying eigenfunction given by,

$$p(\Gamma,t) = \epsilon(1-\mathrm{i})\exp(\pi k t)\sin 2\pi k\Gamma, \tag{1.4a}$$

$$p(\Gamma,t) = \epsilon(1+\mathrm{i})\exp(-\pi k t)\sin 2\pi k\Gamma. \tag{1.4b}$$

Since there are short-wavelength solutions having arbitrarily large growth rates ('Kelvin–Helmholtz instability'), the linearized initial-value problem is not well-posed in the sense of Hadamard (Garabedian 1964). We recall that the classical example of this situation is the problem of analytic continuation, i.e. the initial-value problem for the Cauchy–Riemann equations. For analytic Cauchy data, the Cauchy–Riemann equations have a unique local solution which does not necessarily depend continuously on the data. In line with this analogy, Birkhoff (1962) conjectured the local existence of an analytic solution to the nonlinear problem (1.2). This was proved by Sulem *et al.* (1981). Another conjecture of Birkhoff & Fisher (1959) was that an analytic solution of (1.2) can stop being analytic at a finite time $t_c > 0$. Support for this was given by Moore (1984, 1979) in an asymptotic analysis which predicted that, to leading order in the initial amplitude ϵ, a singularity forms in the vortex sheet at a critical time $t_c(\epsilon)$. The singularity which appears is an infinite jump discontinuity in the vortex sheet's curvature. Using Taylor series in time, Meiron, Baker & Orszag (1982) obtained results in agreement with Moore's.

This recent work has led to a better understanding of vortex-sheet evolution, in contrast to the confusion surrounding the failure of standard numerical methods to solve (1.2). We shall now briefly survey the large literature on these computations; see also Pullin (1982), Moore (1981), Saffman & Baker (1979) and the references contained therein.

1.2. *The point-vortex approximation*

The classical approach to the numerical solution of the initial-value problem (1.2), introduced by Rosenhead (1931), is to replace the curve $z(\Gamma,t)$ by a finite number of points corresponding to a uniform Γ-mesh. Thus $z_j(t)$ approximates $z(\Gamma_j,t)$ for $\Gamma_j = (j-1)\Delta\Gamma, j = 1,\ldots,N$, where $N = 1/\Delta\Gamma$ is the number of points per wavelength. The integral on the right side of (1.2a) is approximated by a simple quadrature rule

which omits the infinite contribution due to the integrand's singularity at $\bar{\Gamma} = \Gamma$. This discretization yields a system of ordinary differential equations for the points' paths:

$$\frac{\mathrm{d}\bar{z}_j}{\mathrm{d}t} = \frac{1}{2\mathrm{i}N} \sum_{\substack{k=1 \\ k \neq j}}^{N} \cot \pi(z_j - z_k), \tag{1.5a}$$

$$z_j(0) = \Gamma_j + p(\Gamma_j, 0). \tag{1.5b}$$

Equation (1.5a) also describes the evolution of N periodic rows of equal strength point vortices and (1.5b) is a common method of initialization in which the point vortices interpolate the initial vortex sheet (1.2b). The term 'vortex sheet' refers to the exact solution of the initial-value problem (1.2), as opposed to an approximating curve constructed from the numerical solution of (1.5). Equations (1.5a) are a Hamiltonian system for the conjugate variables $x_j N^{-\frac{1}{2}}$, $y_j N^{-\frac{1}{2}}$ where $x_j + \mathrm{i}y_j = z_j$; the Hamiltonian function is given by,

$$H_N(t) = \frac{-1}{4\pi N^2} \sum_{j=1}^{N} \sum_{k>j} \ln\left(\cosh 2\pi(y_j - y_k) - \cos 2\pi(x_j - x_k)\right). \tag{1.6}$$

If one assumes that the variables $y_j(t)$ remain bounded, then the invariance of $H_N(t)$ implies that the point vortices remain separated. Numerical computations do not contradict the assumption and we shall accept its validity, as have previous investigators, together with the implication that for each value of N, the ordinary differential equations possess an analytic solution for all time.

By analogy to the flat, constant-strength vortex sheet, (1.5) have the equilibrium solution, $z_j(t) = \Gamma_j$. An analysis, due to von Kármán (Lamb 1932), shows that the linearized discrete problem has perturbation solutions $p_j(t) = z_j(t) - \Gamma_j$ proportional to $\exp 2\pi(\omega t + \mathrm{i}kj/N)$ for $k = 0, 1, \ldots, \frac{1}{2}N$, when the discrete dispersion relation

$$\omega^2 = \tfrac{1}{4}k^2\left(1 - \frac{k}{N}\right)^2 \tag{1.7}$$

is satisfied. For fixed k, these discrete growth rates converge as $N \to \infty$ to the continuous problem's linear growth rates (1.3), a check on the discretization's consistency with (1.2a). Consider (1.5a) in the form, $\mathrm{d}\boldsymbol{X}/\mathrm{d}t = \boldsymbol{F}(\boldsymbol{X})$, $\boldsymbol{X}(0) = \boldsymbol{X}_0$, where $\boldsymbol{X} = (x_1, \ldots, x_N, y_1, \ldots, y_N)$ is the vector of point positions, $\boldsymbol{F}(\boldsymbol{X})$ is the velocity field and $\boldsymbol{X}_0$ is the discrete equilibrium solution. It follows that the Jacobian matrix $(\partial \boldsymbol{F}/\partial \boldsymbol{X})(\boldsymbol{X}_0)$ has eigenvalues $\lambda = \pm 2\pi\omega(k)$ for $\omega(k)$ given by (1.7). The initial condition (1.5b) used in a computation is a perturbation of $\boldsymbol{X}_0$ and at least for a short time, the system's eigenvalues (which are always real and symmetric about zero) will lie approximately in the interval $(-0.25N\pi, 0.25N\pi)$. The term 'stiff' is usually applied to a system of ordinary differential equations for which $\partial \boldsymbol{F}/\partial \boldsymbol{X}$ has large-magnitude eigenvalues with negative real parts (Gear 1971). However for (1.5), the Jacobian matrix also has large real positive eigenvalues and the numerical considerations appropriate for stiff systems do not apply. Accuracy is the prime concern in the present situation, a point we shall return to later.

Using a transverse sinusoidal initial perturbation, Rosenhead integrated the real and imaginary parts of (1.5) by Euler's method with $N = 12$ and a time step $\Delta t = 0.05$. The interpolating curve that was drawn through the points indicated smooth roll-up around periodic concentrations of vorticity. The validity of these findings was challenged by Birkoff (1962) who viewed Rosenhead's work as inconclusive since convergence of the discretization had not been demonstrated. Birkhoff's calculations,

using $N = 20$, fourth order Runge–Kutta time integration and various initial conditions, produced irregular point motion, i.e. smooth roll-up did not occur. Since the appearance of Birkhoff's work, it has become widely accepted that the point-vortex approximation does not converge as $N \to \infty$ and that it is inadequate for studying vortex-sheet evolution.

1.3. *Other numerical work*

Later investigators have sought to repair the presumed defects in the point-vortex approximation and two approaches have emerged:

(i) higher-order accurate discretizations of the integrodifferential equation were derived,

(ii) the integrand in (1.2a) was smoothed by convolution with a cut-off function.

An example of the first approach is the work of van de Vooren (1980), in which the Cauchy-principal-value integral in (1.2a) is replaced by an equivalent integral whose integrand has a removable singularity. The trapezoidal rule is then applied yielding a system of equations which differs from (1.5a) only in the addition of a correction term to the right-hand side,

$$\frac{\mathrm{d}\bar{z}_j}{\mathrm{d}t} = \frac{1}{2\mathrm{i}N} \sum_{\substack{k=1 \\ k \neq j}}^{N} \cot \pi(z_j - z_k) + \frac{1}{4\pi \mathrm{i} N} \left(\frac{z_{\Gamma\Gamma}}{z_\Gamma^2} \right)_{\Gamma = \Gamma_j}. \tag{1.8}$$

The order of accuracy is determined by the approximation used for the Γ-derivatives in the correction term. With an eighth-order finite-difference formula for these derivatives and values of N up to 80, van de Vooren's calculations yielded irregular point motion. A pseudospectral method for calculating the Γ-derivatives in (1.8), proposed by Conte (1979), also led to irregular motion. Other higher-order discretizations of (1.2a) have been proposed (e.g. Higdon & Pozrikidis 1985; Pullin 1982; Baker 1980; Fink & Soh 1978). A variety of numerical procedures has been tried including smoothing techniques. Some calculations have included stabilizing physical effects such as stable density stratification, and surface tension. In spite of these efforts, irregular motion has occurred for the present problem as the number of computational points was increased. Some investigators have presented results which used a small enough number of points to avoid the appearance of irregular motion. Birkhoff's criticism of Rosenhead's work also applies to these investigations; if convergence cannot be demonstrated as the discretization is refined, then conclusions about the vortex sheet are open to doubt.

The second approach is exemplified by the vortex-blob method of Chorin & Bernard (1973), originally applied to a finite vortex sheet. Later applications of the method were reviewed by Leonard (1980). Anderson (1985) has recently applied the method to an interface problem for weakly stratified flow. Vortex-blob calculations for the present problem will appear elsewhere (Krasny 1986).

Moore (1981) pointed out that, with respect to the integrodifferential equation (1.2a), the correction term in (1.8) is the leading-order of the truncation error in the point-vortex approximation. Note that this will be true as long as the Γ-derivatives in the correction term remain bounded, i.e. before the vortex sheet's critical time. However, convergence of the point-vortex approximation at the expected rate $O(N^{-1})$ has not been proved or even demonstrated numerically for any $t > 0$. Moore (1981) used discrete Fourier analysis to study the point-vortex approximation for a circular vortex sheet and found that irregular point motion corresponds to linear modes growing at a rate which agrees with the discrete dispersion relation. He demonstrated

that the onset of this irregular motion could be delayed by using various techniques: linear smoothing (Longuet-Higgins & Cokelet 1976) or repositioning (Fink & Soh 1978). However, the effect of these techniques upon the approximation's accuracy is questionable.

The present work seeks to study singularity formation in a vortex sheet by obtaining accurate numerical solutions to the point-vortex equations (1.5) for a range of values of N and then extrapolating to the limit $N \to \infty$. The first step will be to understand better the source of the irregular point-vortex motion that has been observed by previous investigators. Van de Vooren (1980) attributed the irregular motion to roundoff errors in the computed solution of the point-vortex equations. Birkhoff & Fisher (1959) claimed that the irregular motion was a property of the exact solution of the point-vortex equations. In §2 we show that each of these views is partially correct, i.e. there are two types of irregular motion which can occur in the numerical solution of the point-vortex equations. These are,

(i) a type which occurs at smaller times $t > 0$ as the value of N increases,

(ii) a type which occurs only for times $t > t_c$ (the vortex sheet's critical time) regardless of the value of N.

Computations exhibiting the first type of irregular motion are inaccurate solutions to the ordinary differential equations (1.5). This computational error is not caused by the time-integration method. Its source is instead the computer's finite precision arithmetic which spuriously introduces perturbations at the amplitude of the roundoff error. Once introduced, the perturbations grow according to the equations' dynamics, leading to inaccuracy in the form of irregular point motion. This is consistent with Moore's (1981) findings for the circular vortex sheet, but unlike that work, we emphasize the effect of roundoff error. The first type of irregular point motion would not be present if the computation was performed in exact arithmetic. The approach taken here to abating the difficulty is to use higher precision arithmetic or alternatively, a new filtering technique.

Section 3 is a study of singularity formation in a vortex sheet for which the initial perturbation is a linear-theory-growing eigenfunction of small amplitude/wavelength ratio. The accurate numerical solutions of the point-vortex equations that we obtain do not exhibit irregular motion for $t \leqslant t_c$. The numerical evidence indicates that the point-vortex approximation converges as $N \to \infty$ for $t \leqslant t_c$. We did not observe convergence with increasing values of N for $t > t_c$, when the genuine point-vortex dynamics become more complicated (we have called this the second type of irregular point motion). Extrapolating our results to the limit $N \to \infty$, we find agreement with Moore (1979, 1984) and Meiron *et al.* (1982) on the nature of the singularity that forms in the vortex sheet. A new finding is that for large enough initial amplitude, two singularities appear at the critical time. The results are discussed in §4.

2. Numerical solution of the point-vortex equations

2.1. *The first type of irregular point motion*

To illustrate the first type of irregular point motion, the point-vortex equations (1.5) were solved with $N = 50$ by the fourth-order Runge–Kutta method using the time step $\Delta t = 0.01$ for $t \leqslant 0.25$ and $\Delta t = 0.001$ for $t > 0.25$. The initial condition was a discretized linear theory growing mode of amplitude $\epsilon = 0.01$ and wavelength 1 (see (1.4*a*), (1.5*b*)):

$$z_j(0) = \Gamma_j + 0.01(1 - \mathrm{i}) \sin 2\pi\Gamma_j. \tag{2.1}$$

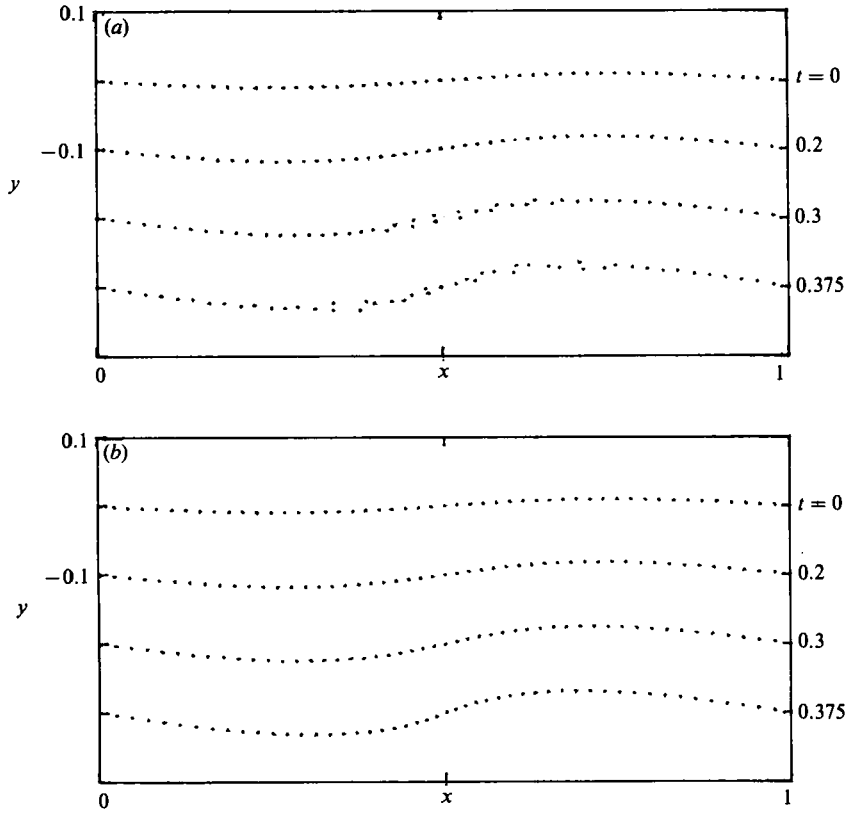

FIGURE 1. Numerical solution of the point-vortex equations (1.5) with initial condition (2.1) using fourth-order Runge–Kutta integration ($N = 50$, $\Delta t = 0.01$ for $t \leqslant 0.25$ and $\Delta t = 0.001$ for $t > 0.25$), (*a*) single precision (7 decimal digits); (*b*) double precision (16 decimal digits). Solution is plotted at $t = 0$, 0.2, 0.3, 0.375.

The calculation was performed on a VAX 11/780 computer in both single-precision (7 decimal digits) and double-precision (16 decimal digits) arithmetic. The computed point positions are shown at successive times for each case in figure 1. In the single-precision calculation, irregular point motion occurs past $t = 0.2$. The point positions at $t = 0.3$ and $t = 0.375$ are very inaccurate solutions of the point-vortex equations with initial condition (2.1). The inaccuracy is not due to time integration error; it was checked that such irregular point motion occurs even if a different time step or integration method is used. In addition, the computed Hamiltonian (1.6) is quite flat over the time interval plotted, with minimum $H_{50}(0.329) = 0.0208013617$ and maximum $H_{50}(0.120) = 0.0208013989$. By contrast, the double-precision results in figure 1 (*b*) have no irregular point motion for $t \leqslant 0.375$ (the subsequent evolution will be discussed later). In this computation, the computed Hamiltonian varied between the values $H_{50}(0) = 0.020801382274\,6$ and $H_{50}(0.375) = 0.020801382277\,4$. By varying the time step it was checked that the point positions in figure 1 (*b*) approximate the solution of the ordinary differential equations to well within the plotting resolution.

Insight into the effect of machine precision is gained by plotting the spatial frequencies of the computed solution. The function $p(\Gamma, t) = z(\Gamma, t) - \Gamma$ is periodic in Γ and the computed quantities $p_j(t) = z_j(t) - \Gamma_j$ are approximations to $p(\Gamma, t)$ at the

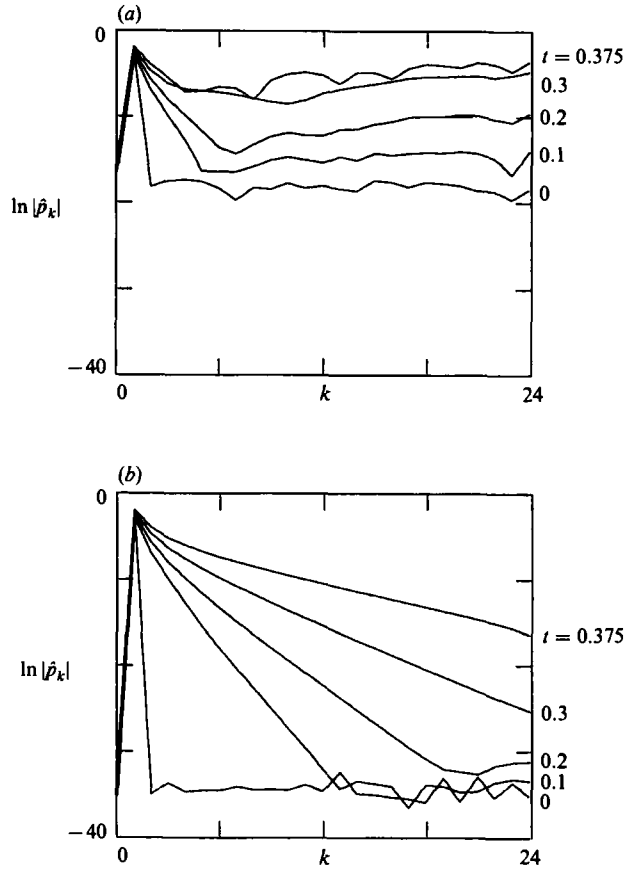

FIGURE 2. Log–linear plots of the Fourier coefficients' (2.2) amplitudes versus wavenumber for the calculations shown in figure 1, (*a*) single precision; (*b*) double precision. The plotted times are $t = 0$, 0.1, 0.2, 0.3, 0.375.

equally spaced points Γ_j. It is therefore natural to consider approximate Fourier coefficients of $p(\Gamma, t)$ defined by

$$\hat{p}_k(t) = N^{-\frac{1}{2}} \sum_{j=1}^{N} p_j(t) \exp(-2\pi i k \Gamma_j) \tag{2.2}$$

for $|k| \leqslant \frac{1}{2}N$, which are obtained in practice by a fast Fourier transform. For the calculations shown in figure 1, the Fourier coefficients' logarithmic amplitudes are plotted in figure 2 as a function of wavenumber at successive times. The initial perturbation in (2.1) has, for $k \geqslant 0$, only one non-zero Fourier coefficient whose amplitude is $|\hat{p}_1(0)| = \epsilon(\frac{1}{2}N)^{\frac{1}{2}}$. Figure 2 shows that the computed initial spectrum contains this spike at $k = 1$ and also contains numerical noise in the higher modes. This noise in the initial condition amounts to a spurious perturbation of the desired initial condition (2.1) and it appears in both calculations at an amplitude determined by the roundoff error.

As time progresses in the single-precision calculation (figure 2*a*), the low-wavenumber modes (approximately $k \leqslant 5$) increase in amplitude, but they remain monotone decreasing in k for each time. The higher-wavenumber modes (approximately $k > 5$) also increase in amplitude as time progresses, but for each fixed

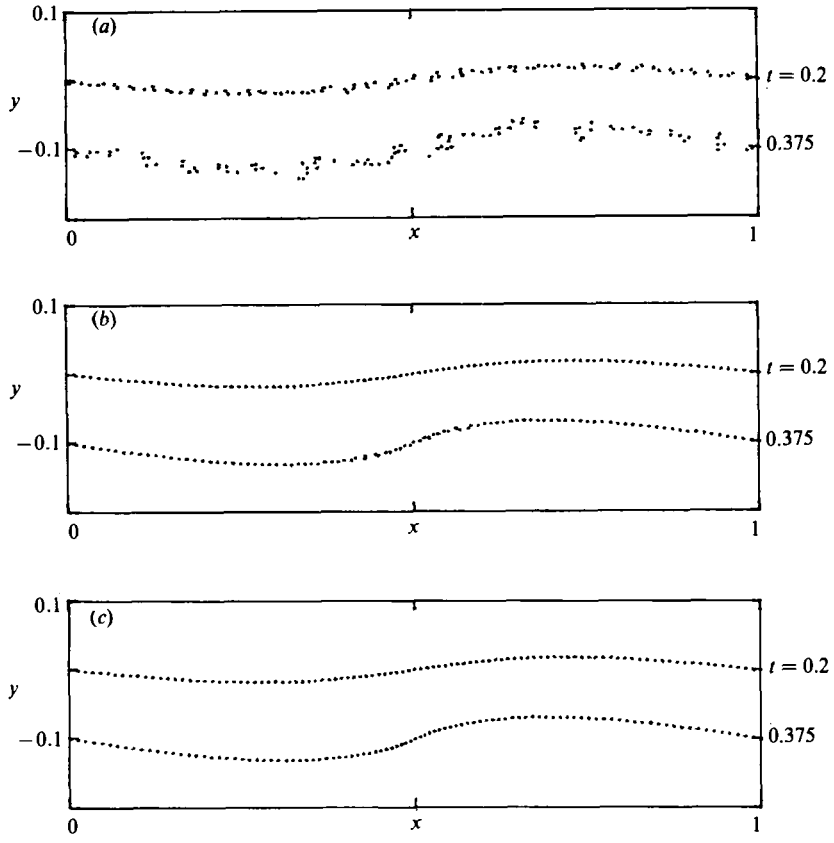

FIGURE 3. Numerical solution of the point-vortex equations (1.5) with initial condition (2.1) using fourth-order Runge–Kutta integration ($N = 100$, $\Delta t = 0.01$ for $t \leqslant 0.25$ and $\Delta t = 0.001$ for $t > 0.25$), (*a*) single precision (7 digits); (*b*) double precision (16 digits); (*c*) CDC double precision (29 digits). Solution is plotted at $t = 0.2, 0.375$.

time, their amplitudes roughly increase with wavenumber. Moore's (1981) finding for the circular vortex sheet also applies here; this growth in amplitude of the high-wavenumber modes is explained by the discrete linear dispersion relation (1.7) and corresponds to the irregular point motion in the physical space plots of figure 1 (*a*).

For the double-precision calculation (figure 2*b*), the higher-wavenumber modes are introduced through nonlinearity rather than through roundoff-error perturbations. At each time, the amplitudes are monotone decreasing as a function of wavenumber; a small amount of growth due to spurious roundoff-error perturbations does occur for $t \leqslant 0.2$ and $k \approx k_{\max}$, but its effect on this computation is insignificant. Even though these higher-wavenumber modes attain larger amplitude as time progresses, there is no sign of small-scale irregular motion in the corresponding point positions (figure 1*b*).

Figures 3 and 4 show the point positions and computed spectra for a calculation with $N = 100$. Results using 7 and 16 digit arithmetic are presented, as well as a 29 digit calculation which was performed using double-precision arithmetic on a CDC 7600 computer. In the 7 and 16 digit calculations, irregular point motion appears sooner with $N = 100$ than it did with $N = 50$. However, it does not appear in the 29 digit calculation. The spectral plots shown in figure 4 further illustrate the idea

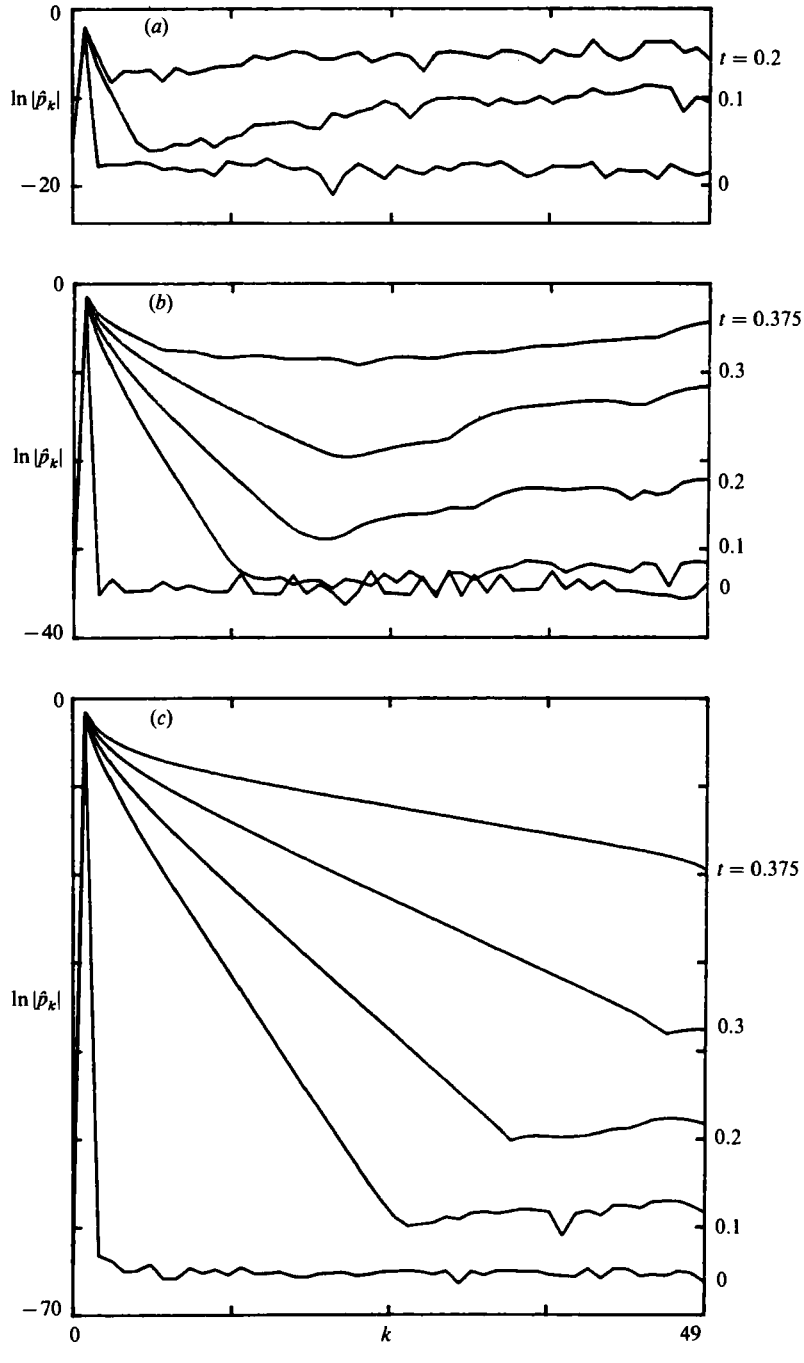

FIGURE 4. Log–linear plots of the Fourier coefficients' (2.2) amplitudes versus wavenumber for the calculations shown in figure 3, (*a*) single precision (7 digits); (*b*) double precision (16 digits); (*c*) CDC double precision (29 digits). The plotted times are $t = 0.0, 0.1, 0.2, 0.3, 0.375$. The last two times are omitted from (*a*) for clarity.

that high wavenumber Fourier modes can grow once they have been spuriously introduced by roundoff error.

2.2. *The effect of machine precision*

For a well-posed linear initial-value problem, Lax's equivalence theorem ensures convergence of a consistent, stable difference scheme (Richtmyer & Morton 1967). In such a situation, roundoff errors may accumulate with each arithmetic operation, but individual perturbations are not amplified in time and they usually do not affect the computational accuracy. There are different numerical considerations for an ill-posed initial-value problem (John 1959). Figures 1–4 demonstrate that machine precision can significantly affect the computational accuracy for the present problem. This phenomenon is subtle and we pause here to consider it more thoroughly.

In the computation, one solves difference equations which come from discretizing the ordinary differential equations in time. If the amplitude of the spurious roundoff-error perturbations is too large, then the computer will not return an accurate solution to the difference equations. The difficulty arises because the initial-value problem (1.2) is ill posed and therefore, to be consistent, the difference scheme must be unstable (see Richtmyer & Morton 1967 p. 59). However, as noted by John (1982), 'Instability of a difference scheme under small perturbations does not exclude the possibility that in special cases the scheme converges towards the correct function, if no errors are permitted in the data or the computation'. This remark appears in the context of a different problem but I believe that it applies also to the present situation. Numerical evidence to be presented in the next section indicates that the point-vortex approximation is a convergent discretization up to the time that the vortex sheet stops being analytic. A computation will exhibit this convergence only if the effect of roundoff error is diminished. The remainder of this section will consider two ways of accomplishing this: higher precision arithmetic, and a filtering technique.

Let 10^{-d} be the roundoff unit and let t_1 be the time at which the first type of irregular motion becomes noticeable. A crude estimate for t_1 is the time at which the fastest-growing linear mode, perturbed by roundoff error at $t = 0$, attains a large amplitude, say 10^{-2}. Using the dispersion relation (1.7), this yields

$$t_1 = \frac{(d-2)}{N} \frac{4 \ln 10}{\pi}. \tag{2.3}$$

This expression qualitatively explains some of the phenomena that were seen in figures 1–4. The first type of irregular point motion will not appear if the value of N is sufficiently small. For a fixed machine precision, using a larger number of points incurs a greater computational error. This is because with more points, shorter wavelengths are represented and once spuriously perturbed by roundoff error they amplify quicker, leading to a faster collapse of the computation. With a fixed number of points, the computational error is reduced by using higher machine precision since that introduces the spurious perturbations at a lower amplitude. The machine precision that is necessary to keep the first type of irregular point motion from appearing increases with N and this method of maintaining computational accuracy is impractical for $N > 100$.

In the present situation, the restriction on the value of N that is imposed by machine precision can be overcome. Moore (1981) used a smoothing technique to control irregular point motion, but a different approach is adopted here. In keeping to the objective of the present work, which is to study singularity formation in

the vortex sheet, we want to examine carefully how the approximation's genuine high-wavenumber component grows, without smoothing it unnecessarily. We next introduce a filtering technique whose goal is to achieve accurate computation with a large value of N without having to use higher machine precision.

2.3. *A filtering technique*

Motivated by the knowledge that the vortex sheet remains analytic for a finite time (Sulem *et al.* 1981), we intend to bias the computation in a particular way. The problem posed here by machine precision is one of 'aliasing' between the discretization of an analytic function and the discretization's computer representation. When an analytic function is interpolated at equidistant points in exact arithmetic, the discrete Fourier coefficients decay exponentially (at least) with increasing wavenumber, but due to roundoff error, the spectrum seen by the computer may not decay. This is shown in the spectral plots (figures 2 and 4) at $t = 0$ where the computational modes for $k > 1$ are present at a finite amplitude even though from (2.1), their exact value is zero. A computational 'noise' level is determined by the machine representation of the initial condition's spectrum and we propose setting to zero, at the end of every time step, any Fourier coefficient whose amplitude is less than this noise level. The point positions will then be correspondingly adjusted by an inverse Fourier transform and the calculation can proceed to the next time step. In order for a mode to grow, its amplitude must jump above the noise level in a single time step and once this has happened for every mode, the filter turns off and the computation proceeds normally.

The technique was used in a 16 digit calculation with $N = 100$ and the same time-stepping as before. The filter level was set to 10^{-13} and in this case, the filter turned off at $t \approx 0.35$. The resulting point positions and Fourier coefficients are plotted in figure 5. In this calculation the Hamiltonian was also well conserved. There is no sign of the first type of irregular point motion which had appeared at $t = 0.375$ in the unfiltered 16 digit calculation (figure 3*b*). The point positions are very close to those of the unfiltered 29 digit calculation (figure 3*c*). There is no spurious growth of Fourier modes as had occurred in figure 4(*b*) since the filter prevented the numerical noise from growing above the horizontal line in figure 5(*b*) (at amplitude $\ln 10^{-13} \approx -30$). The filter does not suppress the growth of the high-wavenumber modes but instead allows them to enter the computation legitimately, through nonlinear effects. Above the computational noise level, the spectra in figure 5(*b*) from the filtered 16 digit calculation agree closely with the spectra from the unfiltered 29 digit calculation (figure 4*c*).

Figure 6 shows the point positions at $t = 0.375$ using $N = 200$ for unfiltered 7, 16 and 29 digit calculations and also for a filtered 16 digit calculation. The 7 and 16 digit results are quite inaccurate and even the 29 digit result exhibits irregular point motion. This motion however is absent from the filtered calculation.

Technically, the filter can be called a smoothing operation since it averages the point positions (in a solution dependent way). However, the aim (and we believe the effect) of the filter is to ensure computational accuracy rather than to smooth or stabilize the calculation. Smoothing, accomplished by convolution in either wavenumber or physical space with a rapidly decaying function, is an alternative approach to the numerical solution of the present ill-posed initial-value problem (Krasny 1986). The filter used here is an *ad hoc* attempt to comply with John's injunction, quoted above, that the data and the computation be free of error. The numerical evidence indicates that, at the expense of introducing a small systematic error, the filter

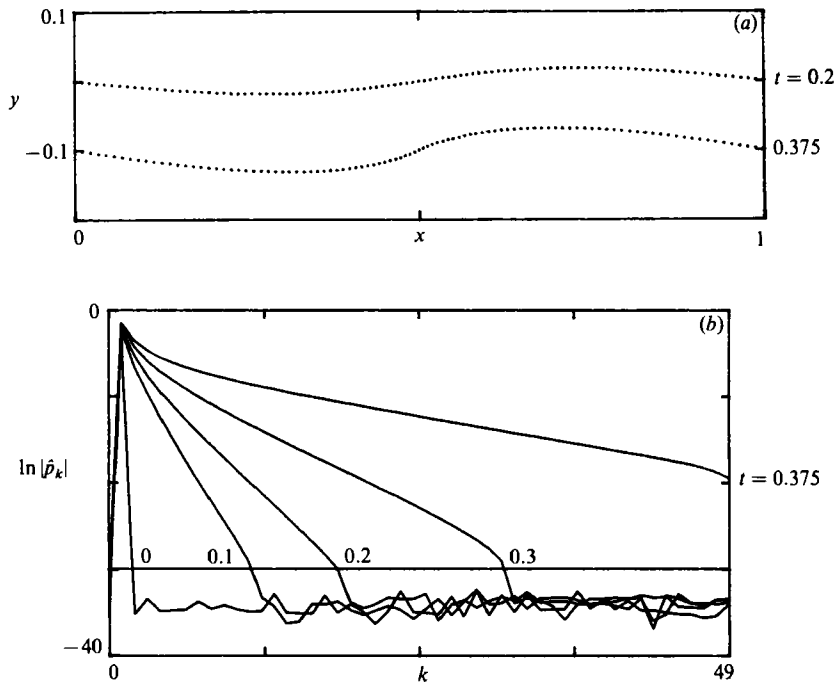

FIGURE 5. Double-precision (16 digit) calculation with the filter level set at 10^{-13} (the horizontal line in (*b*)). This calculation used $N = 100$ and the same time stepping as before, (*a*) point-vortex positions; (*b*) log–linear plot of the Fourier coefficients' (2.2) amplitudes versus wavenumber. Compare this with the unfiltered and the higher precision calculations in figures 3 and 4.

effectively stops spurious roundoff error perturbations from growing for a short time and thus, for a given machine precision, it permits accurate computations with a larger number of points. The error introduced by filtering depends on the filter level and the time step, but this has not yet been rigorously analysed. In the next section when $N > 50$, we will filter using 16 digit arithmetic, instead of less expensive 7 digit arithmetic, since then the filter level can be set lower. Although the filter level can be set even lower in a 29 digit calculation, we have not found the extra expense to be justified since the computed point positions would not be significantly affected.

2.4. *The second type of irregular point motion*

Figure 7 extends figure 1 (*b*) and shows the point positions (with $N = 50$) at several times past $t = 0.375$. The time step has been taken small enough to ensure that the computed point positions are accurate solutions to the ordinary differential equations (1.5) to within the plotting resolution. The two points nearest $\Gamma = 0.5$ approach the central point, pass each other vertically at $t = 0.44$, achieve their minimum separation at $t = 0.446$ and then move apart. At later times there is a central region of rapidly rotating points which grows by capturing pairs of slowly moving points from the outer region as time progresses. In the last panel of figure 7, a straight line interpolating curve of the point positions at $t = 0.5$ has self-intersections.

As t approaches 0.446 it becomes more difficult to maintain a given accuracy in the time integration. To better appreciate the timescales involved, we examined the eigenvalues λ of the Jacobian matrix for the point-vortex equations (recall the discussion in the paragraph following (1.7)). The matrix elements are known

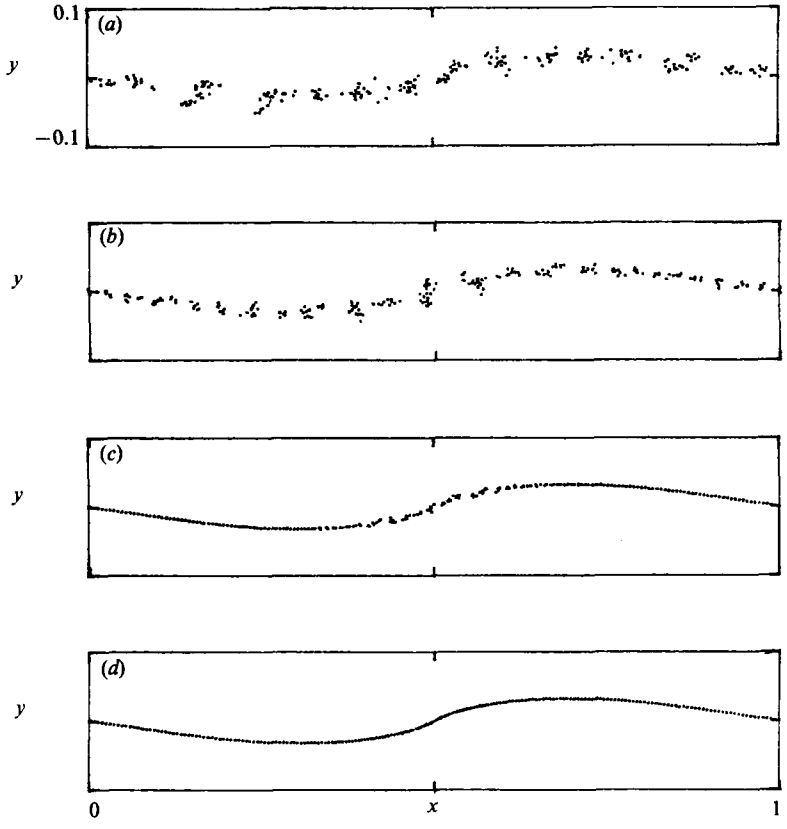

FIGURE 6. Point-vortex positions at $t = 0.375$ for $N = 200$, (*a*) single precision (7 digits); (*b*) double precision (16 digits); (*c*) CDC double precision (29 digits); (*d*) filtered at level 10^{-13}, double precision (16 digits).

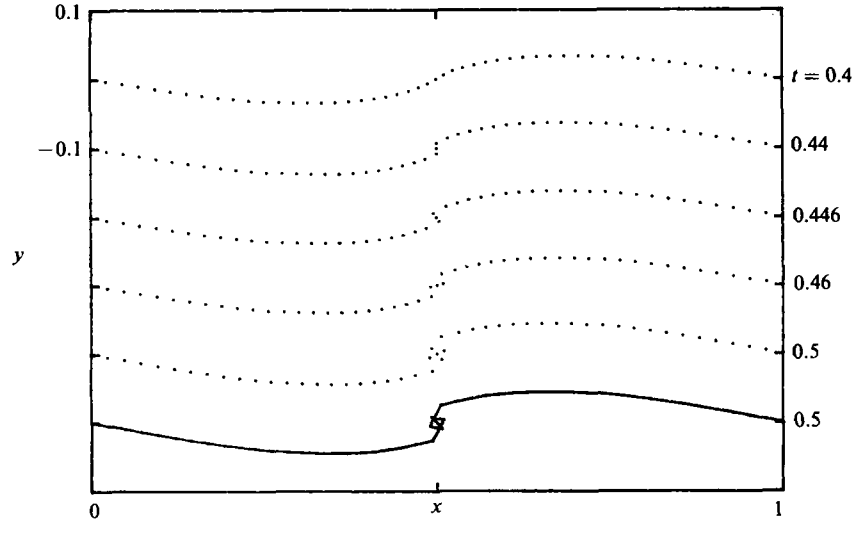

FIGURE 7. Point-vortex positions ($N = 50$) at $t = 0.4$, 0.44, 0.446, 0.46 and 0.5 (extension of figure 1*b*). The last panel is the straight-line interpolant at $t = 0.5$.

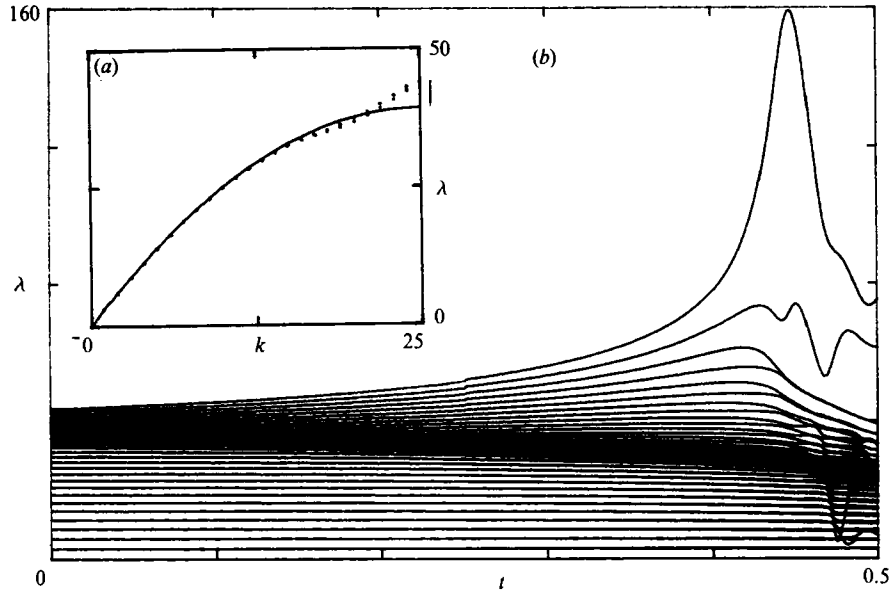

FIGURE 8. Positive eigenvalues λ of the Jacobian matrix of the point-vortex equations with $N = 50$. (a) The curve is a graph of the discrete linear dispersion relation (1.7) corresponding to linearization around the equilibrium point positions. The points are the computed eigenvalues for initial condition (2.1). (b) The eigenvalues' evolution in time.

explicitly and the eigenvalues can be computed by a standard technique once the point positions are supplied. Recall that the eigenvalues are real and symmetric about zero; only the positive eigenvalues will be displayed. The curve in figure 8(a) is the graph of $2\pi\omega(k)$, the discrete dispersion relation (1.7), and the dots are the computed eigenvalues at $t = 0$. It follows from von Kármán's analysis that the eigenvalues for an infinitesimal perturbation lie on the curve and have multiplicity two (except for $\lambda = 2\pi\omega(\frac{1}{2}N)$ which has multiplicity one). The finite initial perturbation amplitude ($\epsilon = 0.01$) moves the large-magnitude eigenvalues away from the curve and causes them to have multiplicity one. Figure 8(b) shows the eigenvalues' evolution in time. For $t < 0.446$ most of the eigenvalues decrease in amplitude. A small number of the large eigenvalues increase; the largest one varies between a value of about 40 at $t = 0$ and about 160 at $t = 0.446$. Associated with the increasing eigenvalues are rapidly varying solution components whose accurate integration has led us to use smaller time steps for $t > 0.25$. For $t \geqslant 0.446$ the situation becomes more complicated as some eigenvalues apparently change multiplicity.

The motion of the point vortices in figure 7 is what we referred to in §1 as the second type of irregular point motion. It will be shown in the next section that $t_c \approx 0.375$ so that this irregular point-vortex motion occurs beyond the vortex sheet's critical time. We emphasize that this is the genuine point-vortex motion for $N = 50$; its relevance to vortex-sheet evolution will be discussed later.

It was found that the onset of the second type of irregular point motion and self-intersections in the interpolating curve, could be delayed by increasing the time-integration error. As expected, such calculations do not conserve the Hamiltonian to as many significant digits, but the actual behaviour was surprising. Figure 9 shows the computed Hamiltonian for the present calculation (extended to $t = 1$) as well as with using fourth order Runge–Kutta integration with $\Delta t = 0.04$ and first-order Euler

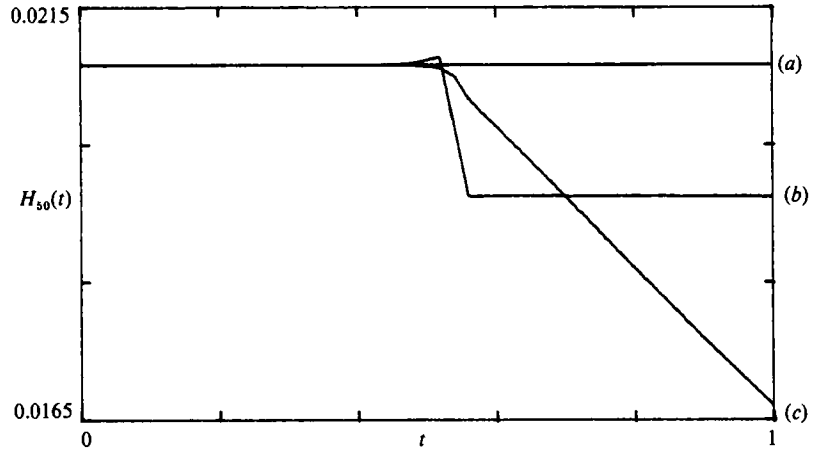

FIGURE 9. Hamiltonian values $H_{50}(t)$ computed up to $t = 1$ using (*a*) fourth-order Runge–Kutta, $\Delta t = 0.01$ for $t \leqslant 0.25$ and $\Delta t = 0.001$ for $t > 0.25$; (*b*) fourth-order Runge–Kutta, $\Delta t = 0.04$; (*c*) first order Euler, $\Delta t = 0.02$.

integration with $\Delta t = 0.02$. In the latter two cases, H_{50} is well conserved until an abrupt change occurs between $t = 0.4$ and $t = 0.6$. In the Runge–Kutta calculation, the Hamiltonian first rises slightly and then jumps to a lower value on which it remains to great accuracy. In the Euler calculation, the Hamiltonian decays continuously. Of course, these variations in H_{50} can be made smaller by decreasing the time step, as shown by the flat line in figure 9(*a*). We shall not pursue the interesting question of why the time discretization affects the Hamiltonian system of point vortices in this particular way.

3. Singularity formation in the vortex sheet

3.1. *Previous investigations*

Singularity formation in the vortex sheet may be studied by exploiting the relation between the complex singularities of $p(\Gamma, t) = z(\Gamma, t) - \Gamma$ and the asymptotic behaviour of its Fourier coefficients (Carrier, Krook & Pearson 1966). Suppose that $p(\Gamma, t)$ can be analytically continued for complex values of Γ to a strip of width $\delta(t)$ in the upper half plane and that a branch point of order $\beta(t) - 1 > -1$ lies on the boundary, i.e.

$$p(\Gamma, t) \approx (\Gamma - (\Gamma_0 + \mathrm{i}\delta(t))^{\beta(t)-1}. \tag{3.1}$$

Then the Fourier coefficients decay as $k \to \infty$,

$$|\hat{p}(k, t)| \approx k^{-\beta(t)} \mathrm{e}^{-k\delta(t)}. \tag{3.2}$$

As the solution evolves in time, the complex singularity traces out a curve in the complex plane (Sulem, Sulem & Frisch 1983). At the critical time, determined by $\delta(t_c) = 0$, the Fourier coefficients' algebraic decay rate $\beta_c = \beta(t_c)$ can be used to infer the regularity of $p(\Gamma, t_c)$.

Previous investigations have used various methods to approximate the Fourier coefficients. Moore's (1984, 1979) asymptotic analysis, based on a transverse sinusoidal initial perturbation,

$$z(\Gamma, 0) = \Gamma - \mathrm{i}\epsilon \sin 2\pi\Gamma, \tag{3.3}$$

predicted that to leading order in the initial amplitude ϵ, a branch point intersects $\Gamma = 0.5$ on the real axis at a critical time given by,

$$\pi t_c + 1 + \ln(2\pi t_c + e^{-2\pi t_c} - 1) = \ln\frac{2}{\pi\epsilon}. \tag{3.4}$$

(To express Moore's results in the present units, replace his z, Γ, ϵ, t by $2\pi(z-\frac{1}{2})$, $2\pi(\Gamma-\frac{1}{2})$, $2\pi\epsilon$, $2\pi t$.) At the critical time the Fourier coefficients' algebraic decay rate is $\beta_c = 2.5$. Meiron *et al.* (1982) applied Moore's analysis to a flat sheet with perturbed strength,

$$z(\Gamma, 0) = e(\Gamma), \quad \Gamma = e + \epsilon \sin 2\pi e. \tag{3.5}$$

They also noted that the particular form of (3.5) allows the exact temporal Taylor series coefficients to be computed. Analysis of these series over a range of initial amplitudes yielded critical times in good agreement with Moore's asymptotic relation for $t_c(\epsilon)$. A value of $\beta_c = 2.7 \pm 0.2$ was obtained for the Fourier coefficients' decay rate. As noted by Moore and Meiron *et al.*, a decay rate of $2 < \beta_c < 3$ is evidence that at the critical time, the sheet's first derivative is continuous although the curvature is infinite at some point. Both investigations found that at the critical time the vortex sheet's y-coordinate is a single-valued function of its x-coordinate. In addition, the sheet's slope remains bounded and the vortex-sheet strength, though continuous, possesses a cusp.

Higdon & Pozrikidis (1985) presented numerical calculations for initial condition (3.5) using a second-order accurate discretization of the integral in (1.2a) and a point insertion technique. Convergence at the rate claimed was not demonstrated and the calculations used a small enough number of points so that irregular motion did not occur. The critical time, taken as the time at which the computed curvature became infinite, was larger than that of Meiron *et al.* although the qualitative dependence on ϵ was similar. There was disagreement with Moore and Meiron *et al.* on the nature of the singularity. Higdon & Pozrikidis claimed that at the critical time, the vortex sheet has the shape of an exponential spiral and the vortex-sheet strength is infinite at the spiral's centre. A Fourier coefficient decay rate of $\beta_c = 2.3 \pm 0.2$ was quoted but no explanation was offered of how this can be consistent with the presence of an exponential spiral in the sheet's shape.

We have applied Moore's (1984) analysis to the linear theory growing eigenfunction of amplitude ϵ,

$$z(\Gamma, 0) = \Gamma + \epsilon(1-i)\sin 2\pi\Gamma, \tag{3.6}$$

and found the critical time relation,

$$\pi t_c + 1 + \ln \pi t_c = \ln\frac{1}{2\pi\epsilon}. \tag{3.7}$$

The critical time in (3.4) for the transverse sinusoidal initial perturbation is greater than that in (3.7) by an amount (≈ 0.2) which does not vanish as $\epsilon \to 0$. This delayed critical time is plausible since the perturbation in initial condition (3.3) contains both a growing and a decaying linear theory eigenfunction of amplitude $\frac{1}{2}\epsilon$ (see (1.4)).

In the remainder of this section we use the point-vortex method to study singularity formation in the vortex sheet with initial condition (3.6). The first step will be to obtain estimates of the critical time which are based on solutions to the point-vortex equations for several values of N. We shall then extrapolate to the limit $N \to \infty$ and compare this with the results of the previous investigations.

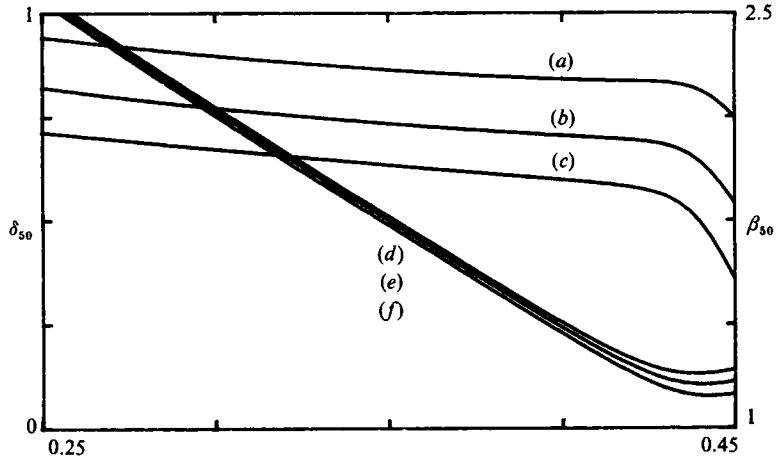

FIGURE 10. Least-squares estimates of $\delta_{50}(t)$ and $\beta_{50}(t)$ for $0.25 \leqslant t \leqslant 0.45$ based on the $N = 50$ calculation (figure 2*b*) for several fitted ranges of wavenumbers, (*a*) $\beta(2 \leqslant k \leqslant 10)$; (*b*) $\beta(3 \leqslant k \leqslant 10)$; (*c*) $\beta(4 \leqslant k \leqslant 10)$; (*d*) $\delta(6 \leqslant k \leqslant 20)$; (*e*) $\delta(5 \leqslant k \leqslant 20)$; (*f*) $\delta(4 \leqslant k \leqslant 20)$. The δ scale is on the left and the β scale is on the right.

3.2. *Extrapolation to the limit* $N \to \infty$

As seen in §2.1, approximate Fourier coefficients for the vortex sheet are available by taking the fast Fourier transform of the computed perturbation quantities. Following Sulem *et al.* (1983) and Brachet *et al.* (1983), in which spectral numerical methods were used to study loss of analyticity in other nonlinear evolution equations, $\delta(t)$ and $\beta(t)$ are estimated by least-squares fitting of the computed spectrum to the model (3.2). Wavenumbers close to $k_{\max}$ are excluded from the fit as are modes with amplitude below the noise level. Figure 2(*b*) indicates the plausibility of expression (3.2) and suggests that a high-wavenumber band be used to estimate $\delta(t)$ and a low-wavenumber band be used for $\beta(t)$. Values of $\delta_{50}(t)$ and $\beta_{50}(t)$, fit to the model (3.2) over several wavenumber ranges, are shown in figure 10 (the subscript denotes an estimate based on $N = 50$ points). Changing the fitted range has a small effect on $\delta_{50}(t)$ as long as a band of high wavenumbers is included. The values of $\delta_{50}(t)$ decrease linearly with time until they fall within a strip above zero. We do not ascribe special significance to the particular values of $\beta_{50}(t)$ since these estimates are sensitive to the band of low wavenumbers used in the fit.

Calculations were performed for eight values of N up to 200. With $N > 50$, the filter level was set to 10^{-13} and the time step ($\Delta t = 0.0002$ in the final portion of the Runge–Kutta integration) was sufficiently small to ensure several digit accuracy in the computed point positions. For all values of N used, the behaviour was qualitatively similar to what has already been presented in figure 10. In particular, $\delta_N(t)$ decreases linearly with time until it falls within a strip of width $O(N^{-1})$. The sensitivity of $\beta_N(t)$ to the range of fitted wavenumbers makes it difficult to estimate β_c this way. Estimates of the critical time could be based on the times at which $\delta_N(t)$ attains its minimum, but we propose two other estimates which are more conveniently computed.

Let t_v^N be the first time at which a point passes vertically over another point and let t_s^N be the time at which the minimum separation $s_{\min}^N$ of any pair of points is attained. The computed values are given in table 1. In all cases it was found that the two points adjacent to $\Gamma = 0.5$ were the ones for which these spatial phenomena

N	t_v^N	t_s^N	$s_{\min}^N \cdot 10^2$	$y_{0.4}^N \cdot 10^2$	$y_{0.49}^N \cdot 10^3$
20	0.526	0.541	2.057	−2.052	−13.15
40	0.455	0.462	0.931	−2.163	−8.701
50	0.44	0.446	0.725	−2.186	−7.694
80	0.417	0.421	0.433	−2.221	−6.105
100	0.4092	0.412	0.355	−2.232	−5.557
120	0.4034	0.406	0.28	−2.24	−5.168
150	0.3976	0.3996	0.221	−2.248	−4.784
200	0.3914	0.3928	0.163	−2.256	−4.409
∞	0.375	0.375	0.01	−2.28	−3.23

TABLE 1. The dependence on N. t_v^N = first time at which a point vortex passes vertically over another point vortex. t_s^N = time of minimum separation of any pair of point vortices. $s_{\min}^N$ = minimum separation between any pair of point vortices. The last two columns contain y-coordinate values at $t_c = 0.375$ for $\Gamma = 0.4$ and $\Gamma = 0.49$. The former are all at point positions and the latter are computed by linear interpolation of adjacent point positions. The values in the last row were obtained by extrapolation to the limit $N \to \infty$ (see figures 11 and 14). The extrapolated value $s_{\min}^\infty$ differs from its exact value zero because of small errors in the computed values of $s_{\min}^N$.

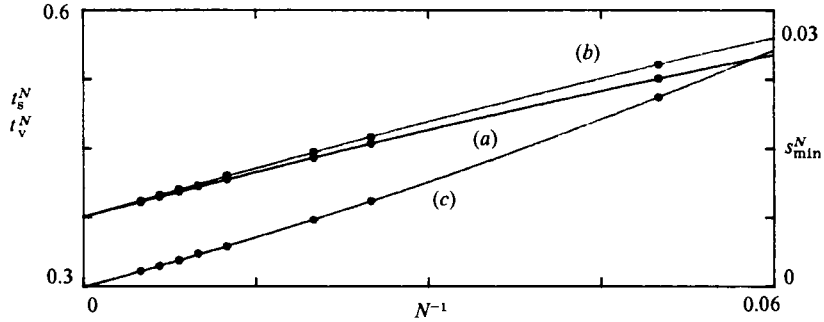

FIGURE 11. Values of (a) t_v^N, (b) t_s^N and (c) $s_{\min}^N$ from table 1 plotted as function of N^{-1}. The curves are quadratic polynomials in N^{-1} whose coefficients are determined by least-squares fitting to the eight data points in table 1. The timescale is on the left and the separation scale is on the right.

occurred ($t_v^{50} = 0.44$ and $t_s^{50} = 0.446$ were plotted in figure 7). The values of t_v^N, t_s^N and $s_{\min}^N$ are plotted as functions of N^{-1} in figure 11 along with the quadratic polynomials in N^{-1} whose coefficients are determined by a least-squares fit to the eight data points. The good fit obtained is evidence of asymptotic convergence in the sense that,

$$t_v^N \approx t_v^\infty + c_1 N^{-1} + c_2 N^{-2} + \dots \quad (N \to \infty), \tag{3.8}$$

(similarly for t_s^N and $s_{\min}^N$). The constant term of the least-squares quadratic polynomial gives a value extrapolated to the limit $N \to \infty$ and appears in the last row of table 1. The extrapolated value $s_{\min}^\infty = 0.0001$ differs from the exact value zero because of small errors in the computed $s_{\min}^N$. For each N, the time t_s^N is greater than t_v^N but both sequences converge to the same limit as $N \to \infty$. We take the extrapolated time $t_v^\infty = 0.375$ as the estimate of the vortex sheet's critical time. This value is less than that (0.45) given by the asymptotic relation (3.7). A comparison between the computed critical time for several initial amplitudes and the asymptotic relation (3.7) will be given later.

Log–log plots of the discrete Fourier coefficients' amplitudes $|\hat{p}_k(t_c)|$ at the critical time $t_c = 0.375$ for $N = 50$, 100 and 200 are shown in figure 12. As the value of N

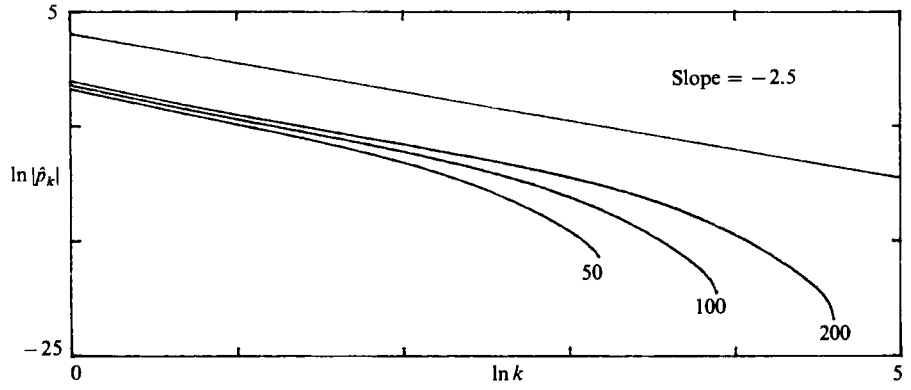

FIGURE 12. Log–log plot of the Fourier coefficients' (2.2) amplitudes at $t_c = 0.375$ for $N = 50$, 100 and 200. The straight line has slope -2.5, the value obtained by Moore (1979).

increases, algebraic decay extends to higher wavenumbers, implying the presence of a singularity in the vortex sheet at that time. This algebraic decay is well described by the straight line in figure 12 which has slope -2.5, the value obtained by Moore.

We turn now to the shape of the vortex sheet at the critical time. Figure 13(*a*) shows the point positions at t_v^N for $N = 50$, 100 and 200. In the enlarged view (figure 13*b*) the points in the interval $0.4 \leqslant \Gamma \leqslant 0.6$ have been connected by a straight-line interpolant. For each value of N, at t_v^N the interpolating curve has a kink, but it does not follow that the vortex sheet also has a kink at the critical time t_v^∞. At time t_v^N the two points adjacent to $\Gamma = 0.5$ are connected by a short vertical segment whose length approaches zero as $N \to \infty$. This implies that at the critical time, the vortex sheet's y-coordinate is a single-valued function of its x-coordinate. It was also observed that for fixed time $t \leqslant t_c = 0.375$, the interpolating curves converge as $N \to \infty$, with an error that is an asymptotic series in N^{-1} as in (3.8). Typical values exhibiting this convergence are $y^N(\Gamma = 0.4, t_c)$ and $y^N(\Gamma = 0.49, t_c)$ which are given in table 1 and plotted in figure 14. The point at which the singularity forms $z(\Gamma = 0.5, t) = 0.5$ remains fixed by symmetry. The interpolating curve for $N = 200$ at $t_c = 0.375$, is shown in figure 15. This curve describes the vortex sheet's shape at the critical time. The singularity is not visually apparent in the shape; as in the work of Moore and Meiron *et al.*, the vortex sheet has a bounded slope and shows no sign of roll-up at the critical time.

Values of the vortex-sheet strength ($\sigma = (x_\Gamma^2 + y_\Gamma^2)^{-\frac{1}{2}}$) and curvature ($\kappa = (x_\Gamma y_{\Gamma\Gamma} - y_\Gamma x_{\Gamma\Gamma})\sigma^3$) were computed using backward differences for $\Gamma < 0.5$ and forward differences for $\Gamma > 0.5$. The values at $\Gamma = 0.5$ were taken to be the average of the adjacent values. For $t < t_c$ both σ and κ were smooth functions of Γ with the strength having a maximum at $\Gamma = 0.5$ and the curvature changing sign there. Values of σ and κ along the curve at t_c for $N = 50$, 100 and 200 are plotted in figure 16. The results indicate the presence at $\Gamma = 0.5$ of a cusp in the vortex-sheet strength and a jump discontinuity in the curvature. Note that these features of the vortex sheet do not appear for any particular discrete approximation but only emerge in the limit $N \to \infty$. As mentioned above, the Fourier coefficients' decay rate $\beta_c \approx 2.5$ suggests that the curvature jump in the vortex sheet is infinite. The computed maximum values of the sheet strength in figure 16(*a*) increase with N. In view of the first-order convergence of the computed sheet positions and the divergence of the sheet's second derivative at $\Gamma = 0.5$, there is reason to doubt that a finite-difference approximation

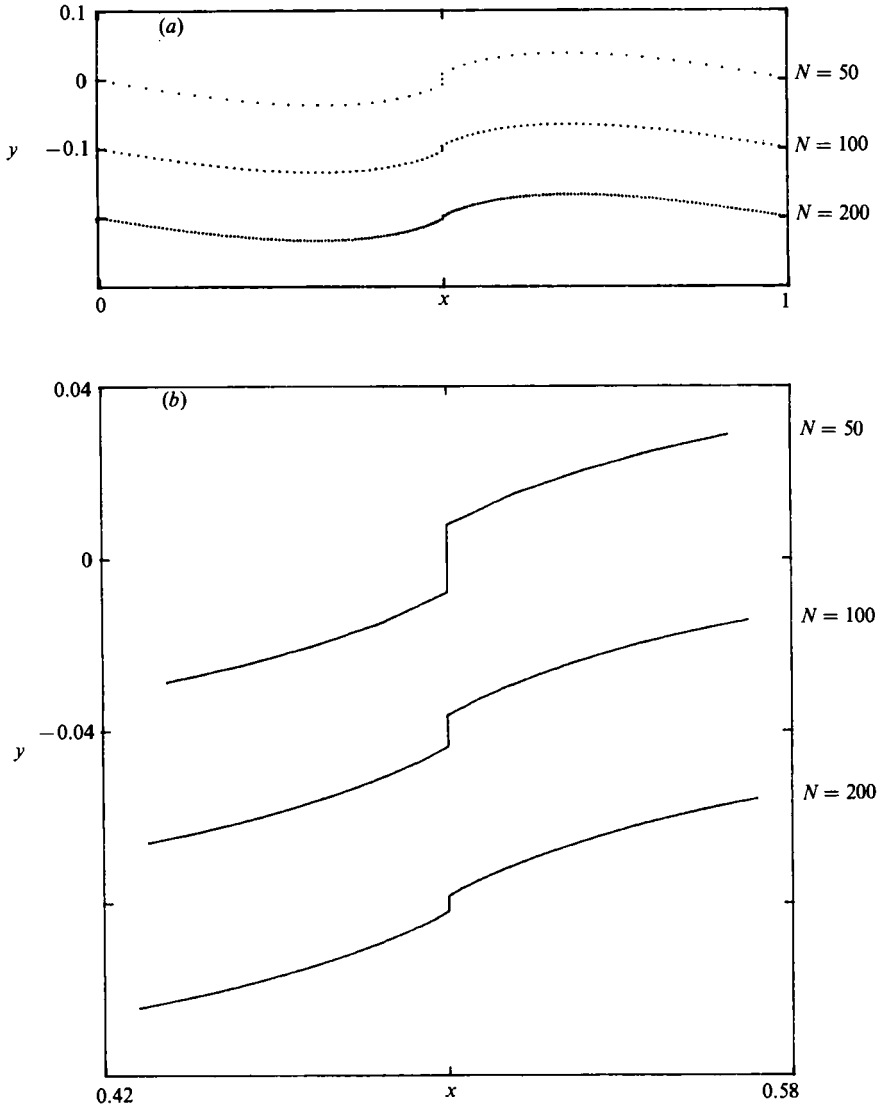

FIGURE 13. (*a*) Point vortex positions at t_v^N for $N = 50, 100, 200$; (*b*) closeup of the straight-line interpolant of the point positions for $0.4 \leqslant \Gamma \leqslant 0.6$.

for $\sigma(\Gamma = 0.5, t_c)$ is reliable for determining whether the cusp's amplitude is finite or infinite. To resolve this issue we examine the Fourier coefficients of the computed vortex-sheet strength at t_c. Log–log plots in figure 17 show that these Fourier coefficients decay algebraically at a rate close to 1.5, an indication that the vortex-sheet strength has a cusp of finite amplitude.

In spite of differences in the initial condition and methodology, the description of singularity formation obtained here agrees with that of Moore (1984, 1979) and Meiron *et al.* (1982). As previously mentioned, Higdon & Pozrikidis (1985) obtained a different description of the singularity. However, they presented calculations using only two different sets of mesh parameters and were unable to examine the limit as their discretization is refined. Their conclusions therefore describe two particular approximating curves whose relevance to the vortex sheet is unclear.

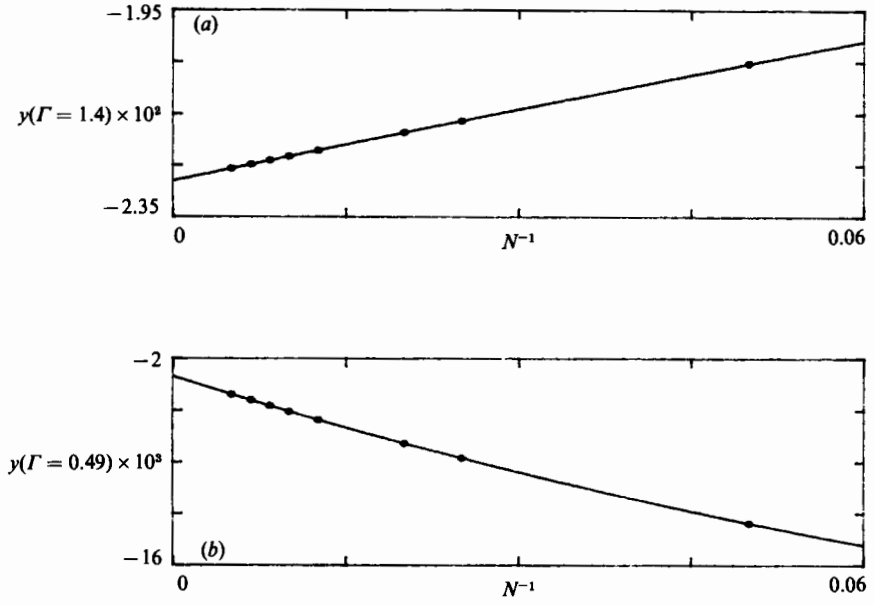

FIGURE 14. Values of the computed y-coordinates from table 1 plotted as functions of N^{-1}. (*a*) $y^N(\Gamma = 0.4, t_c = 0.375) \cdot 10^2$; (*b*) $y^N(\Gamma = 0.49, t_c = 0.375) \cdot 10^3$. The curves are quadratic polynomials in N^{-1} whose coefficients are determined by least-squares fitting to the eight data points in table 1. The y-coordinates in (*a*) are point positions and those in (*b*) are computed by linear interpolation of adjacent point positions.

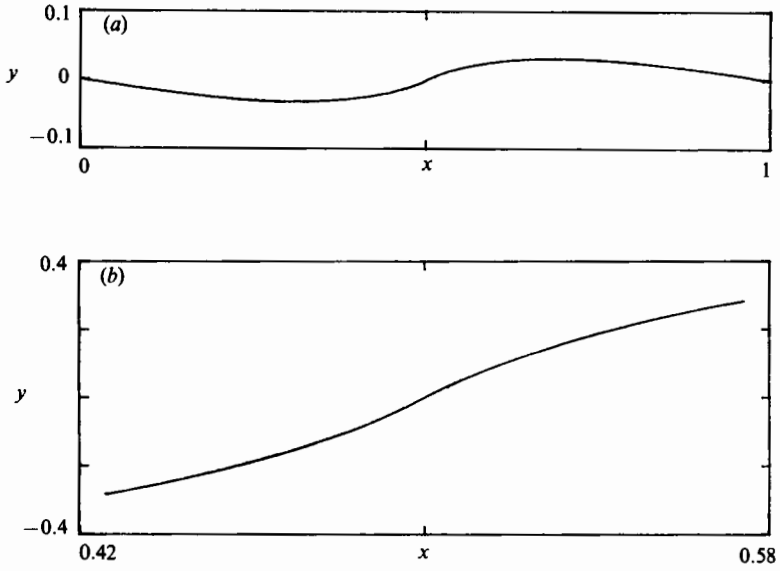

FIGURE 15. (*a*) Straight line interpolating curve for $N = 200$ at $t_c = 0.375$. This curve describes the vortex sheet's shape at the critical time. (*b*) Closeup for $0.4 \leqslant \Gamma \leqslant 0.6$.

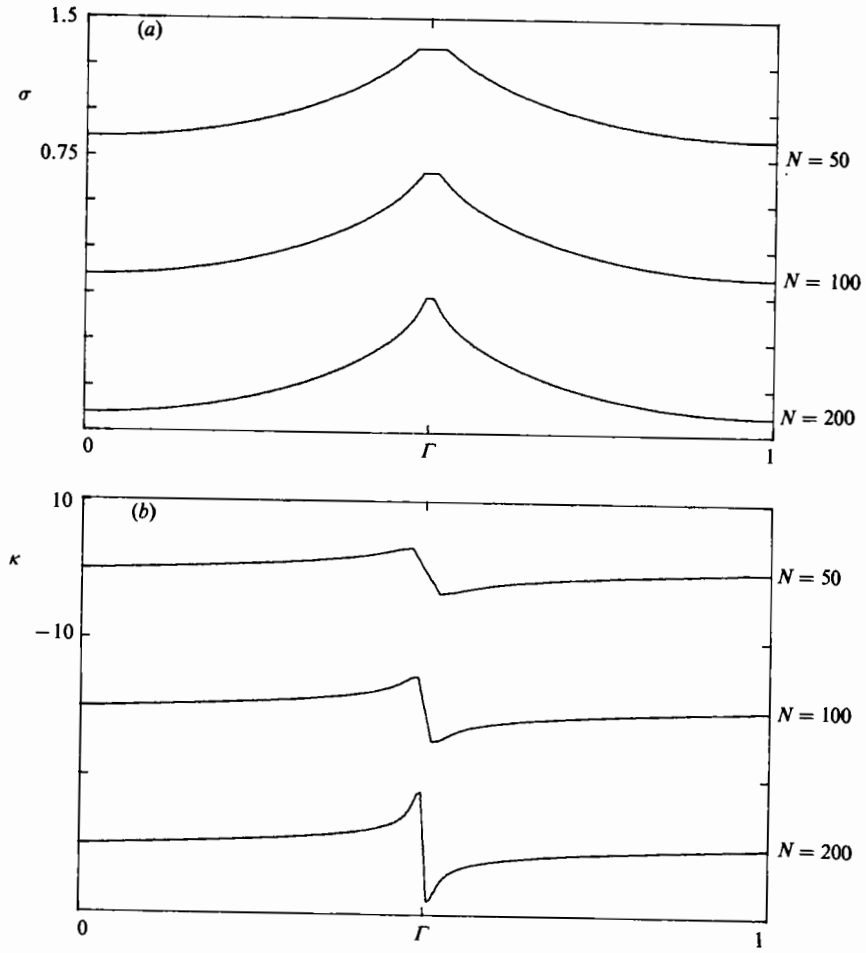

FIGURE 16. Solution at $t_c = 0.375$ for $N = 50$, 100 and 200. (a) vortex-sheet strength σ. (b) sheet curvature κ.

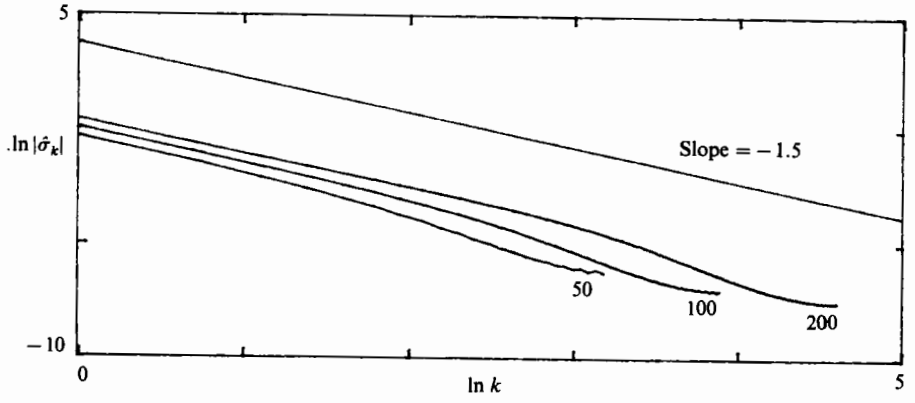

FIGURE 17. Log–log plot of the Fourier coefficients' amplitudes for the computed vortex-sheet strength in figure 16(a). The straight line has slope −1.5.

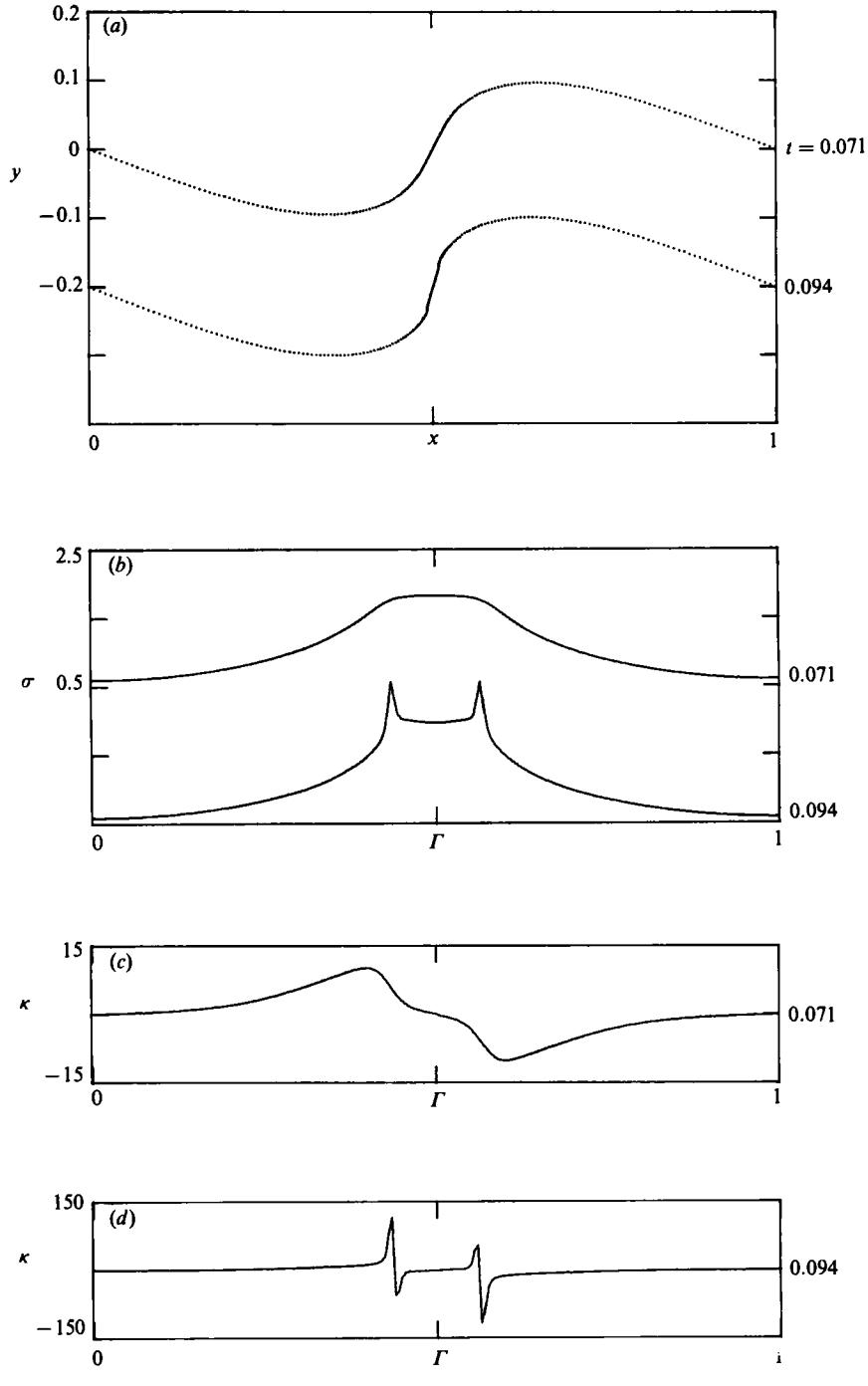

FIGURE 18. Calculation with $\epsilon = 0.08$ using $N = 200$, plotted at times $t = 0.071$ and $t_v^{200} = 0.094$, (*a*) point-vortex positions; (*b*) vortex-sheet strength σ; (*c*) curvature κ at $t = 0.071$; (*d*) curvature κ at $t_v^{200} = 0.094$.

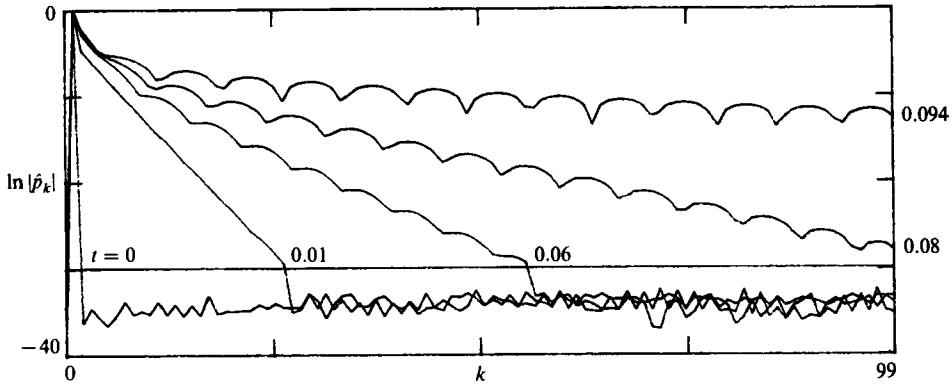

FIGURE 19. Log–linear plots of the Fourier coefficients' (2.2) amplitudes versus wavenumber for the solution plotted in figure 18. Plotted times are $t = 0$, 0.01, 0.06, 0.08, 0.094.

N \ ϵ	0.000625	0.00125	0.0025	0.005	0.01	0.02	0.04	0.08
50	1.28	1.08	0.88	0.7	0.52	0.36	0.22	0.12
100	1.18	0.99	0.8	0.62	0.46	0.31	0.19	0.11
200	1.115	0.93	0.75	0.58	0.425	0.285	0.175	0.105
∞	1.04	0.86	0.695	0.54	0.385	0.26	0.16	0.1

TABLE 2. The dependence of the critical time on the initial amplitude. Values of t_v^N are given. These computations used Euler's method with $\Delta t = N^{-1}$. Two levels of Richardson extrapolation were used to obtain the critical time estimates in the last row. All times are rounded to within 0.005.

3.3. *The dependence on initial amplitude*

The results presented thus far have used $\epsilon = 0.01$ for initial condition (3.6). Results using smaller initial amplitude are qualitatively similar, the difference being that the critical time is larger and the vortex sheet's maximum slope and amplitude at that time are smaller. Larger initial amplitude produces a significant difference as shown in figure 18 for which $\epsilon = 0.08$. At $t = 0.071$, the points near $\Gamma = 0.5$ lie on an almost straight short-line segment of constant strength. At $t_v^{200} = 0.094$ there are two places along the curve at which points are passing each other vertically. These two places correspond to maxima in the sheet strength and to jumps in the curvature. The Fourier coefficients (2.2) of the vortex sheet shown in figure 19 contain a modulation of the basic behaviour (3.2), a sign that two branch points are present. These results suggest that the singularity appearing at $\Gamma = 0.5$ for small initial amplitude bifurcates to two singularities at a certain finite initial amplitude. Pozrikidis & Higdon (1985) found a similar phenomenon in the dynamics of constant vorticity layers, in that the layer thickens and rolls up at two places if the initial perturbation amplitude is large enough.

Since studying the critical time's dependence on ϵ requires many separate computations, it is desirable to use a less costly time-integration method instead of the fourth-order Runge–Kutta method with small time steps that was used until now. With Euler's method the total truncation error is $O(N^{-1}) + O(\Delta t)$ and the two terms can be balanced by choosing $\Delta t = N^{-1}$. Using this time stepping, values of t_v^N were computed as before with initial amplitudes in the range $0.0006125 \leqslant \epsilon \leqslant 0.08$ for

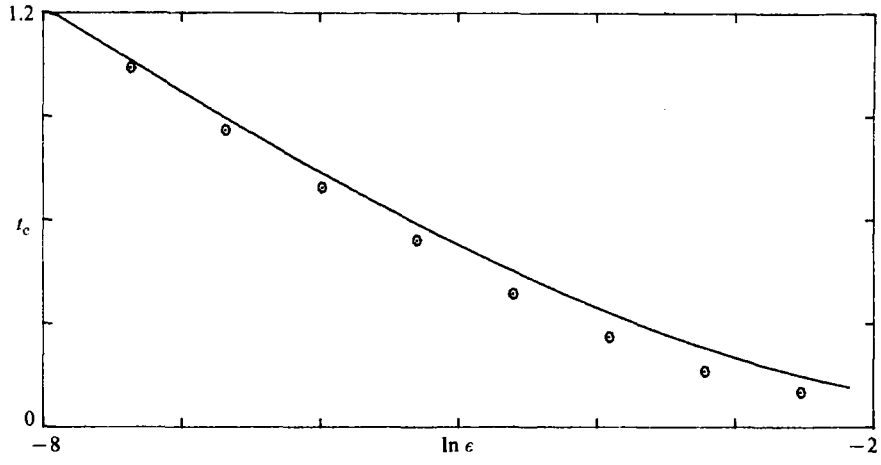

FIGURE 20. The dependence of the critical time on the initial amplitude. The circles are the extrapolated values from table 2. The curve is the asymptotic relation (3.7) derived using Moore's (1984) procedure.

$N = 50$, 100 and 200 (table 2). Two levels of Richardson extrapolation were applied to obtain the critical-time estimates in the last row of table 2 (the values are rounded to within 0.005). For $\epsilon = 0.01$ the critical time obtained here is 0.385, in reasonable agreement with the previous value 0.375, considering the values of N and Δt used. Figure 20 shows that there is good agreement between these computed critical times and the asymptotic relation (3.7) derived using Moore's procedure.

4. Closing remarks

Rosenhead's point-vortex approximation for vortex-sheet evolution from periodic analytic initial data has been examined. Our findings pertain to two issues: the accurate numerical solution of the point-vortex ordinary differential equations, and the nature of singularity formation in the vortex sheet.

The numerical integration of the point-vortex equations, with the initial condition given by discretizing an analytic curve, is subject to difficulties. Due to the ill posedness of the underlying continuous problem, the difference scheme is unstable and therefore, spurious spatial perturbations introduced by roundoff error can lead to inaccuracy in the form of irregular point motion. This phenomenon may also occur in computations for other ill-posed initial-value problems e.g. Rayleigh–Taylor instability (Baker, Meiron & Orszag 1980). In order to control this source of computational error, which becomes more severe as the number of points increases, we have introduced a filtering technique which suppresses the growth of the spurious roundoff-error perturbations for a short time. Analyticity is important for the filter's effectiveness – we know *a priori* that the exact solution remains analytic for a finite time and this should be reflected by a rapid decay of the discretization's Fourier coefficients. Another key ingredient is that the roundoff error, which is invisible at small times in physical space, shows up clearly in wavenumber space. The numerical evidence indicates that a filtered computation differs little from an unfiltered computation performed using higher machine precision, although more work is needed to establish conditions for the filter's rigorous validity.

Apart from this difficulty arising due to roundoff error and instability of the

difference scheme, there is the difficulty of maintaining a given accuracy in the time integration. In a neighbourhood of the vortex sheet's critical time, a small number of point vortices develop sharply faster timescales. Accordingly, the fourth-order Runge–Kutta method and time-step reduction were used when the goal was to maintain high accuracy in the time integration. Since our main concern was the vortex sheet, rather than the evolution of any particular finite number N of point vortices, a less-expensive alternative strategy was also proposed for $t \leqslant t_c$, namely to integrate the point-vortex equations by the first order Euler method with $\Delta t = N^{-1}$ and then to extrapolate to the limit $N \to \infty$.

The numerical evidence presented indicates that the point-vortex approximation converges as $N \to \infty$, up to the vortex sheet's critical time. Numerical vortex methods have been proven convergent for flows with smooth vorticity (see Anderson & Greengard 1985; Beale & Majda 1982; Cottet 1982; Hald 1979). Supplying a convergence proof in the present case is an area for future work. Our results indicate that for $t \leqslant t_c$, the error in the point-vortex approximation behaves like an asymptotic power series in N^{-1}. Since the operation count per time step is $O(N^2)$, this has the important practical consequence that improved accuracy can be obtained by extrapolating the results based on several moderate values of N rather than using a single expensive computation with a large value of N. This approach should be contrasted with the higher-order-accurate discretizations of the integral in (1.2a) which have been proposed by other investigators (e.g. Higdon & Pozrikidis 1985; van de Vooren 1980; Baker 1980; Fink & Soh 1978). These discretizations assume a degree of differentiability in the vortex sheet which is not present at the critical time. For example, van de Vooren's correction term in (1.8) is infinite for $\Gamma = 0.5$ when $t = t_c$. In other words, these discretizations lose their consistency at the vortex sheet's critical time. This explains part of the difficulty in converging that these methods have experienced with the present problem. Higher-order methods are also subject to the roundoff error difficulty for certain mesh sizes. Were it not for the singularity formation, using progressively higher-order-accurate discretizations might be an appropriate alternative for dealing with the roundoff error difficulty (John 1959). This is because a given error tolerance could then be attained using a coarser mesh (with its smaller perturbation growth rates). However, in view of the current lack of a rigorous convergence theory for ill-posed initial-value problems, convergence cannot be taken for granted and it is reasonable to ask that convergence be demonstrated numerically.

The computations presented used a linear-theory-growing eigenfunction of small amplitude/wavelength ratio as the initial perturbation. Our results agree with the findings of Moore (1984, 1979) and Meiron *et al.* (1982) that a singularity forms in the vortex sheet at a finite time. Our estimate for the order of the branch point is not sharp, but it is close to 1.5, the order predicted by Moore's asymptotics. We found that at the critical time the vortex sheet's slope is bounded, the sheet strength has a cusp of finite amplitude and the sheet's curvature is infinite at the singularity. Critical time estimates were obtained whose dependence on the initial amplitude agrees well with the asymptotic relation derived using Moore's procedure. A new finding is the simultaneous formation of two singularities along the sheet for large enough initial amplitude. Properly used, the point vortex approximation is a reliable and efficient tool for studying singularity formation in a vortex sheet and it complements the techniques of Moore and Meiron *et al.* All of these methods are approximate and there remains a need for a rigorous proof of singularity formation.

In our calculations, the interpolating curve developed self-intersections sooner past

t_c with increasing values of N. Pointwise convergence was not observed for $t > t_c$ and therefore, we can draw no conclusions about how (or even if) the vortex sheet evolves past the critical time. We have called the point vortices' behaviour past t_c 'the second type of irregular motion', but it is irregular only in that it does not yield the roll-up expected for the vortex sheet. The point-vortex motion seen here for $t > t_c$ may be related to chaotic dynamics whose presence has been conjectured for large numbers of point vortices (see Aref 1983). The point vortices' behaviour has intrinsic mathematical interest, but for $t > t_c$ it may well be irrelevant to the vortex sheet's evolution. It is emphasized that these comments refer to the exact solution of the point-vortex ordinary differential equations. As already mentioned in §2.4, we found that using a rather large time step, i.e. solving the point-vortex equations less accurately, delayed the appearance of self-intersections in the interpolating curve. Figure 9 indicates that the dynamics of the time-discretized system can be quite different (for $t > t_c$) than the exact point-vortex dynamics. Various time-stepping strategies of the form $\Delta t = CN^{-1}$ (where $C = O(1)$) were investigated but convergence was not observed for $t > t_c$ as $N \to \infty$ meaning that again, no conclusion about the vortex sheet for $t > t_c$ can be justified on the basis of these computations.

Moore (1979) and Meiron *et al.* (1982) felt that singularity formation may represent a restriction on the validity of the vortex-sheet model. However, there are situations in which a weak solution to an evolution equation exists, and is physically relevant, past the time of singularity formation, e.g. shock waves in compressible flow (Lax 1973) and curvature discontinuities in flame fronts (Sethian 1985). The analogous questions for a vortex sheet deserve attention. D. I. Pullin (private communication 1983) has conjectured that for $t > t_c$ the vortex sheet rolls up on both sides of the singularity, forming a double-branched spiral which vanishes in size as $t \to t_c$ from above. Calculations using the vortex blob method (Krasny 1986) are consistent with Pullin's conjecture but more theoretical and computational work on this issue is needed to better assess the validity and usefulness of the vortex-sheet model for describing physical shear-layer dynamics.

I wish to thank my thesis advisor Professor A. J. Chorin and Professors O. H. Hald, G. M. Corcos, L. E. Fraenkel and J. Goodman for helpful discussions and for commenting on early versions of the manuscript. I thank Professors G. Majda and P. D. Lax for useful suggestions. I am grateful to Professor D. W. Moore for a copy of his IUTAM lecture and to Professor J. J. L. Higdon for preprints of his work. I thank the *Journal's* editor, Dr H. E. Huppert for his efforts, and Professor A. J. Roberts and the other referees for pointing out shortcomings in the earlier versions of the paper. The computations were performed at the Lawrence Berkeley Laboratory and the Courant Institute of Mathematical Sciences. This work supersedes my Ph.D. thesis (Krasny 1983) (partially supported by the US Department of Energy under contract DEAC03-76SF00098). I am currently supported by a National Science Foundation Postdoctoral Research Fellowship.

REFERENCES

ANDERSON, C. 1985 A vortex method for flows with slight density variations. *J. Comp. Phys.* **61**, 417.

ANDERSON, C. & GREENGARD, C. 1985 On vortex methods. *SIAM J. Num. Anal.* **22**, 413.

AREF, H. 1983 Integrable, chaotic, and turbulent vortex motion in two-dimensional flows. *Ann. Rev. Fluid Mech.* **15**, 345.

BAKER, G. R. 1980 A test of the method of Fink and Soh for following vortex sheet motion. *J. Fluid Mech.* **100**, 209.

BAKER, G. R., MEIRON, D. I. & ORSZAG, S. A. 1980 Vortex simulations of the Rayleigh–Taylor instability. *Phys. Fluids* **23**, 1485.

BATCHELOR, G. K. 1967 *An Introduction to Fluid Mechanics*. Cambridge University Press.

BEALE, J. T. & MAJDA, A. 1982 Vortex methods 2: Higher order accuracy in two and three dimensions. *Maths. Comp.* **39**, 29.

BIRKHOFF, G. & FISHER, J. 1959 Do vortex sheets roll up? *Rend. Circ. Mat. Palermo ser.* 2 **8**, 77.

BIRKHOFF, G. 1962 Helmholtz and Taylor instability. *Proc. Symp. Appl. Math. XIII A.M.S.* 55.

BRACHET, M. E., MEIRON, D. I., ORSZAG, S. A., NICKEL, B., MORF, R. & FRISCH, U. 1983 Small-scale structure of the Taylor–Green vortex. *J. Fluid Mech.* **130**, 411.

CARRIER, G. F., KROOK, M. & PEARSON, C. E. 1966 *Functions of a Complex Variable*, p. 255. McGraw Hill.

CHORIN, A. J. & BERNARD, P. S. 1973 Discretization of a vortex sheet, with an example of roll-up. *J. Comp. Phys.* **13**, 423.

CONTE, R. 1979 Etude numerique des nappes tourbillonnaires. These, DPh-G/PSRM, CEN. Saclay.

COTTET, G. H. 1982 Ph.D. these. l'Université Pierre et Marie Curie, Paris.

FINK, P. T. & SOH, W. K. 1978 A new approach to roll-up calculations of vortex sheets. *Proc. R. Soc. Lond.* A **362**, 195.

GARABEDIAN, P. R. 1964 *Partial Differential Equations*, p. 109. John Wiley.

GEAR, C. W. 1971 *Numerical Initial Value Problems in Ordinary Differential Equations*. Prentice-Hall.

HALD, O. 1979 The convergence of vortex methods, 2. *SIAM J. Num. Anal.* **16**, 726.

HIGDON, J. J. L. & POZRIKIDIS, C. 1985 The self-induced motion of vortex sheets. *J. Fluid Mech.* **150**, 203.

JOHN, F. 1959 Numerical solution of problems which are not well posed in the sense of Hadamard. *Proc. Rome Symp. Prov. Int. Comp. Center*, 103.

JOHN, F. 1982 *Partial Differential Equations*, 4th ed. p. 8, Springer.

KRASNY, R. 1983 A numerical study of Kelvin–Helmholtz instability by the point vortex method. Ph.D. thesis. Lawr. Berk. Lab. rep. #17092.

KRASNY, R. 1986 Desingularization of periodic vortex sheet roll-up. *J. Comp. Phys.* (to appear.)

LAMB, H. 1932 *Hydrodynamics*. Cambridge University Press.

LAX, P. D. 1973 Hyperbolic systems of conservation laws and the mathematical theory of shock waves. *Reg. Conf. Ser. Appl. Math. SIAM 11.*

LEONARD, A. 1980 Vortex methods for flow simulations. *J. Comp. Phys.* **37**, 289.

LONGUET-HIGGINS, M. S. & COKELET, E. L. 1976 The deformation of steep surface waves on water. 1. A numerical method of computation. *Proc. R. Soc. Lond.* A **350**, 1.

MEIRON, D. I., BAKER, G. R. & ORSZAG, S. A. 1982 Analytic structure of vortex sheet dynamics. 1. Kelvin–Helmholtz instability. *J. Fluid Mech.* **114**, 283.

MOORE, D. W. 1979 The spontaneous appearance of a singularity in the shape of an evolving vortex sheet. *Proc. R. Soc. Lond.* A **365**, 105.

MOORE, D. W. 1981 On the point vortex method. *SIAM J. Sci. Stat. Comput.* **2**, 65.

MOORE, D. W. 1984 Numerical and analytical aspects of Helmholtz instability. *IUTAM lecture.*

POZRIKIDIS, C. & HIGDON, J. J. L. 1985 Non-linear Kelvin–Helmholtz instability of a finite vortex layer. *J. Fluid Mech.* **157**, 225.

PULLIN, D. I. 1982 Numerical studies of surface-tension effects in nonlinear Kelvin–Helmholtz and Rayleigh–Taylor instability. *J. Fluid Mech.* **119**, 507.

ROSENHEAD, L. 1931 The formation of vortices from a surface of discontinuity. *Proc. R. Soc. Lond.* A **134**, 170.

RICHTMYER, R. D. & MORTON, K. W. 1967 *Difference Methods for Initial-Value Problems*. Interscience.

SAFFMAN, P. G. & BAKER, G. R. 1979 Vortex interactions. *Ann. Rev. Fluid Mech.* **11**, 95.

SETHIAN, J. A. 1985 Curvature and the evolution of fronts. *Comm. Math. Phys.* **101**, 4.

SULEM, C., SULEM, P. L., BARDOS, C. & FRISCH, U. 1981 Finite time analyticity for the two and three dimensional Kelvin–Helmholtz instability. *Comm. Math. Phys.* **80**, 485.

SULEM, C., SULEM, P. L. & FRISCH, U. 1983 Tracing complex singularities with spectral methods. *J. Comp. Phys.* **50**, 138.

VAN DE VOOREN, A. I. 1980 A numerical investigation of the rolling up of vortex sheets. *Proc. R. Soc. Lond.* A **373**, 67.